Energy Conversion and Management 139 (2017) 206–221

Contents lists available at ScienceDirect

Energy Conversion and Management

journal homepage: www.elsevier.com/locate/enconman

Design and operational procedures for ORC-based systems coupled with internal combustion engines driving electrical generators at full and partial load

Viorel Badescu [a,b,*], Mahdi Hatf Kadhum Aboaltabooq [c,d], Horatiu Pop [d], Valentin Apostol [d], Malina Prisecaru [d], Tudor Prisecaru [d]

[a] Candida Oancea Institute, Polytechnic University of Bucharest, Spl. Independentei 313, Bucharest 060042, Romania
[b] Romanian Academy, Calea Victoriei 125, Bucharest, Romania
[c] Al-Furat Al-Awsat Technical University, Technical College Najaf, Iraq
[d] Department of Thermodynamics, Engines, Thermal and Refrigeration Equipment, Faculty of Mechanical Engineering and Mechatronics, University POLITEHNICA of Bucharest, Spl. Independentei 313, Bucharest 060042, Romania

ARTICLE INFO

Article history:
Received 6 November 2016
Received in revised form 14 February 2017
Accepted 17 February 2017

Keywords:
Internal combustion engines
Waste heat recovery
Electric generator
Organic Rankine cycle
Partial load

ABSTRACT

This paper refers to recovering waste heat from the hot gases exhausted by internal combustion engines (ICEs) driving electric generators (EGs) at full and partial load. The topic is of particular interest for developing countries where electric grids are underdeveloped or missing and electricity is generated locally by using classical fuels. The heat recovery system is based on an Organic Rankine Cycle (ORC). A novel method is proposed for the optimum design of ORC-based systems operating in combination with ICE at partial EG loads. First, ORC-based systems coupled with ICEs operating at full EG load is treated. Specific results for the operation at full EG load are as follows: (i) the optimum superheating increment ranges between 30 and 40 °C, depending on the type of the working fluids; (ii) a pinch point temperature difference exits between the flue gas temperature and the working fluid at the evaporator inlet; (iii) the total area of the evaporator is very close to the total area of the condenser, a fact which facilitates manufacturing; (iv) the surface area of the preheater zone is about 75% of the total surface area, while those of the boiler zone and superheater zone is about 13.5% and 11.5%, respectively. Second, the case of the ORC-based systems coupled with ICEs operating at partial EG load is considered. Specific results for this case are as follows: (v) the net power may be maximized by optimizing the working fluid mass flow rate; (vi) when the ICE is coupled with an ORC-based system, the overall thermal efficiency of the combined system, $\eta_{ICE\text{-}ORC}$, is higher than the thermal efficiency of the ICE operating alone. As an example, for the case treated here, $\eta_{ICE\text{-}ORC}$ is higher than η_{ICE}, by 6.00%, 5.85% and 5.91%, for EG loads of 100%, 75% and 50%, respectively.

1. Introduction

Electrical energy is the most used form of energy. In developing countries, a wide-spread power grid is lacking and electricity production depends on local electric generators (EG). These generators are usually driven by internal combustion engines (ICE). Approximately 30% to 40% of the fuel energy in ICEs is being converted into useful mechanical work and the rest is residual heat expelled into environment through flue gases and engine cooling systems [1]. Recovery and utilization of this waste heat saves fossil fuels and reduces the amount of heat lost and greenhouse gases released into the environment. Also, the waste heat may be used for electricity generation, by increasing the effectiveness of the combination ICE-EG.

The organic Rankine cycle (ORC) systems are well suited to recover waste heat from sources of low and medium temperature. In Europe, power generation with ORC-based systems of waste heat coming from ICEs is already well established technology and such systems can be found on the market. A number of such systems has been already installed in the recent years in Italy at Pavia (0.6 MWe), Portogruaro (0.6 MWe), Catania (0.6 MWe), Pescara (0.7 MWe), Chivasso (1 MWe), Pisticci (1.8 MWe) and Pisticci Scalo (4 MWe), in Germany at Kempen (0.6 MWe) and Senden (1 MWe) and in Finland at Ammassuo, Espoo (1.3 MWe) [2]. Note that all

* Corresponding author at: Candida Oancea Institute, Polytechnic University of Bucharest, Spl. Independentei 313, Bucharest 060042, Romania.
E-mail address: badescu@theta.termo.pub.ro (V. Badescu).

http://dx.doi.org/10.1016/j.enconman.2017.02.046
0196-8904/

these projects involve rather large installed power (more than 0.5 MWe) and were implemented in industrialized countries, where high level technologies are available. Most situations of practical interest in developing countries refer to smaller installed capacities, of the order of tens of kW. Such a small scale application is considered in this paper.

The performance of coupled ICE – ORC-based heat recovery systems has been studied in several recent studies and important results were reported. They belong to two different themes and are briefly presented next.

Several studies involved first law and second law analysis for the steady state operation of simple ORC configurations, with emphasis on the waste heat recovery from exhaust gas, cooling water or lubricant. Working fluids were also under discussion. Vaja and Gambarotta [3] developed a thermodynamic model with the purpose to efficiently match a vapor cycle to that of a stationary ICE. First, a parametric analysis was conducted in order to determine the optimal evaporating pressures for each fluid. Subsequently, three different cycle setups were considered: a simple cycle using only the engine exhaust gases as a heat source, a simple cycle using the exhaust gases and the engine cooling water and a regeneration-based cycle, respectively. A second law analysis was performed, which demonstrated that 12% increase in the overall efficiency can be achieved with respect to the engine with no bottoming; nevertheless it has been observed that the ORC can recover only a small fraction of the heat released by the engine through the cooling water. A steady-state energy balance and exergy analysis was presented by He et al. [4] for ICE operation. Different characteristics of the waste heat from the exhaust gas, cooling water, and lubricant have been considered. Suitable working fluids to be used in high-temperature ORC were proposed and the performance of a combined thermodynamic cycle has been analyzed. Results showed that more waste heat can be recovered by using the combined cycle, compared with the traditional cycle configuration. Wang et al. [5] analyzed the characteristics of a novel system combining a gasoline engine with a dual loop ORC which recovered waste heat from both the exhaust and coolant systems. A high temperature loop recovered the exhaust heat while a low temperature loop recovered both the residual heat from the high temperature loop and the coolant heat. Results showed that the low temperature loop net power was higher than the high temperature loop net power and the relative output power improved by 14–16% in the peak thermal efficiency region and by up to 50% in the small load region. The overall effective thermal efficiency increased by 3–6%. Boretti [6] studied the recovery of waste heat from exhaust gases and coolants via ORCs. The system was a hybrid vehicle powered by a 1.8 L naturally aspirated gasoline engine. The ORC systems fitted on the exhaust and the coolant lines enabled an increase in the fuel conversion efficiency of up to 6.4% and 2.8% individually, and by up to 8.2% when both ORC systems were considered.

A special interest has been given in literature to different ORC configurations and working fluids to recover heat from exhaust gas and engine coolant. Shu et al. [7] compared the performance of three regenerative dual-loop ORC systems with the performance of a simple ORC system. Waste heat of the exhaust, engine coolant and residual heat of the high temperature (HT) loop was recovered by these four systems. The optimization of the operation parameters was carried out, followed by an irreversibility analysis. Results showed that the low condensation temperature at the HT loop was beneficial for the performance optimization. The inlet turbine temperature in the HT loop should be high for wet fluids in subcritical cycle and low for dry fluids in both subcritical and transcritical cycles. Xi et al. [8] examined the performances of three different ORC systems, including the basic ORC (BORC) system, the single-stage regenerative ORC (SRORC) system and the double-stage regenerative ORC (DRORC) system, using six different working fluids under the same waste heat conditions. The operation of the ORC systems has been optimized for using each working fluid. Results showed that for all working fluids, the DRORC system gave the best thermal and exergy efficiency, followed by the SRORC system, while the BORC system had the poorest efficiency. R11 and R141b were recommended as suitable working fluids for ORC systems, due to their superior thermodynamic performances. Yu et al. [9] presented a simulation model based on an actual ORC bottoming system of a diesel engine. The ORC system was built to recover waste heat both from engine exhaust gas and jacket water using R245fa as a working fluid. Results indicated that, approximately 75% and 9.5% of exhaust gas and jacket water waste heat, respectively, have been recovered under engine conditions ranging from high loads to low loads. The ORC system performed well under the rated engine conditions, with expansion power up to 14.5 kW, recovery efficiency up to 9.2% and exergy efficiency up to 21.7%. Combined with the bottoming ORC system, the diesel engine thermal efficiency was improved by up to 6.1%. Wang et al. [10] studied Rankine cycle-based exhaust energy recovery systems on heavy-duty diesel engines and light-duty vehicle gasoline engines. The influences of evaporating pressure, engine type and load on the system performances were analyzed with multiple objectives, including improving thermal efficiency and reducing CO_2 emissions, the total heat transfer area per net power, the cost of producing electricity and the payback period. Results revealed that higher pressures and engine loads were desirable for better performances. Shu et al. [11] proposed a novel dual-loop ORC, which consisted of a high-temperature loop and a low-temperature loop to recover the exhaust and engine coolant waste heat and the HT loop residual heat. The objective functions were the net power, the utilization rate of the engine coolant, the dual-loop ORC thermal efficiency and the exergy efficiency. Results showed that the maximum net power, utilization rate of the engine coolant and exergy efficiency were 36.77 kW, 96.8% and 55.05%, respectively. For all working fluids, the system performed better at high operating load. R1234yf was found to be a better working fluid for high operating load. R124 exhibited the poorest performance under all operating loads.

The present paper brings two different kinds of original contributions: it covers a new research topic and it comes with several improvements concerning the formal treatment. Few details about these two aspects are presented below.

The short previous review showed that the existing literature is poor in studies related to the utilization of the power generated by ORC-based heat recovery systems from ICEs in driving EGs at partial load. Note that few authors focused on ORC-based heat recovery systems from ICEs operating at partial load [9]. However, their results may be extrapolated to the case of EGs operating at partial loads only when linearity exists between partial loads of ICEs and partial loads of EGs. This linearity is still in need to be proven. Therefore, a major aspect of practical interest in developing countries is considered in this paper, i.e. power generated by ORC-based heat recovery systems from ICEs in driving partial loaded EGs.

The formal treatment brings several original contributions, which are shortly described next. First, the operation conditions were usually defined in a way which is specific to the ICE characteristics (see [9] for instance, where five ICE operation conditions were treated). This makes generalization difficult and prompted us to define the operation regime of the ICE in a more clear way, in terms of the full EG load operation. The performance of ORC-based systems in combination with ICE operating at partial EG load is analyzed here. Second, the models developed in previous studies were based on different scenarios concerning the input data. In this paper an important step forward is made. Input data come from experiments on ICE flue gases temperature and mass flow rate.

Third, a novel ORC design methodology is proposed, which involves two steps. Step one refers to developing a steady state model for waste heat recovery based on energy balance equations. This model enables the determination of the optimum operation of ORC-based systems coupled with partially loaded EGs. The second step involves the design of the heat exchangers geometry, which allows maximum power output. Basically, the design method consists of finding the optimum evaporator pressure and designing the geometry of the evaporator and condenser associated with the maximum net power in correlation with the working fluid. A similar design methodology is presented in [12]. A procedure is proposed here for the operation of the ORC-based system, involving continuous optimization of the working fluid mass flow rate to obtain maximum power.

The paper is organized as follows. First, the experimental setup is presented in Section 2. Section 3 describes the ORC system while the ORC model and its validation are presented in Section 4. Section 5 shows results, including a procedure for the design of ORC systems. Conclusions are listed in Section 6.

2. Experimental setup

The heat recovery from a commercial automotive ICE is considered in this paper. It is a 3.3 L (0.83 L/cylinder), compression ignition, four-cylinder engine located in the Thermal Research Center, Faculty of Mechanical and Mechatronics Engineering, University POLITEHNICA of Bucharest. This ICE is driving an EG manufactured by Yanmar (model type 4TNV98TGGEHR). The experimental setup is shown in Fig. 1.

The engine technical characteristics of the ICE and the fuel specifications are presented in Table 1 [14].

Experimental data measured during the operation of this engine are used as input when the ORC-based system is analyzed. The two major primary sources of waste heat from an ICE are the engine flue gas (medium-grade) and engine coolant (low-grade). Two thermal parameters are of interest. The first parameter is the temperature of flue gas, which is measured after the turbocharger. The second parameter is the water jacket inlet temperature.

In practice, the EG (item #2 in Fig. 1) is coupled with a consumer of electric energy. The electric demand is simulated here by using an electric simulator consisting of six electric heaters equipped with cooling fans and a two-stage adjustment of the electrical load Fig. 2. Each stage means 4.1 kWe. The bench is fitted with an acquisition and data storage system that consists of a programmable logic controller (PLC) connected to a personal computer (PC).

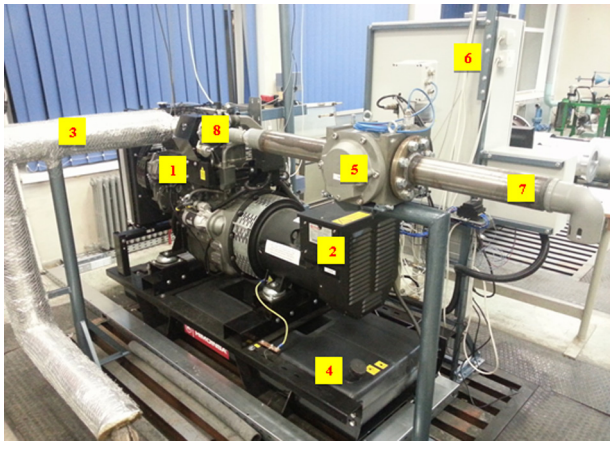

Fig. 1. The experimental setup. 1 – ICE (Diesel engine); 2 – EG (electric generator); 3 – flue gas pipe; 4 – fuel tank; 5 – air flow meter; 6 – automation and data acquisition panel; 7 – air flow pipe and 8- turbocharger [13].

Table 1
Main ICE characteristics [14].

Parameter	Symbol	Specification	Units
Engine type (model)	–	4-Cylinder	–
Power	P_{ICE}	37.7	kW
Piston stroke	S	110	mm
Compression ratio	CR	18:1	–
Lower heating values of fuel	LHV	43	MJ/kg
Flue gas temperature	t_g	289–480	°C
Cylinder diameter	D	98	mm
Rotation speed	ω_n	1500	rpm
Flue gas mass flow rate	$\dot{m}_g$	192.2–192.6	kg/h
Water jacket mass flow rate	$\dot{m}_w$	327.6–1105.5	kg/h

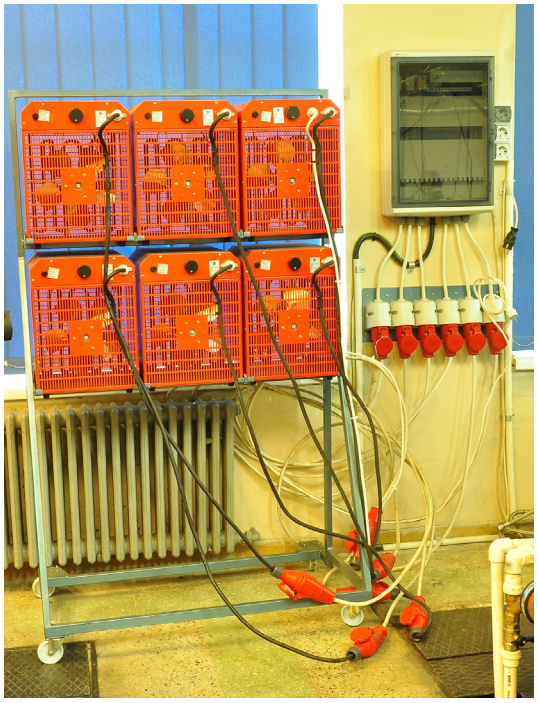

Fig. 2. Electric load simulator.

Experiments are performed at different EG loads (50%, 75% and 100%) at engine rotation speed of about 1500 rpm.

3. Organic Rankine cycle system

The ORC may be coupled to the ICE in different ways, depending on different waste heat sources. Three different configurations for heat recovery from the flue gas of the ICE and from the coolant used by the ICE were analyzed in [15]. The amount of heat recovery and the cycle output power for these configurations depend on their characteristics. The investment is however proportional with the complexity of the configuration. The simplest and less expensive configuration is considered here. It involves heat recovery from flue gas. This choice is justified by the heat recovery potential of the hot flue gas, which is much higher than that of the coolant.

The ORC-based heat recovery system considered in this paper consists of an expander, a condenser, an evaporator (heat recovery unit), a working fluid pump and other auxiliary equipment. As shown in Fig. 3, through process 1–2, the working fluid pressure is increased by the pump, then it enters the evaporator and is converted to saturated vapor by receiving heat from the flue gas (pro-

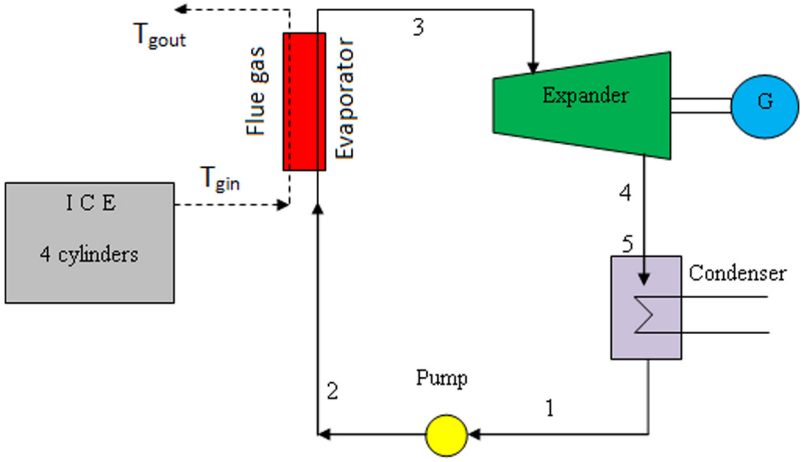

Fig. 3. Simple ICE-ORC configuration.

cess 2–3). The symbols T_{gin} and T_{gout} represent the inlet flue gas temperature to the evaporator and the outlet temperature, respectively. Next, the working fluid enters the expander and generates mechanical power (process 3–4). After the expander, the working fluid enters the water cooled condenser where it is converted into saturated liquid and releases heat (process 4–5). After the condenser, the working fluid re-enters the pump and the operation cycle is repeated.

4. Model

The following basic assumptions are adopted: (i) Steady-state conditions; (ii) No pressure drops in heat exchangers and connecting pipes; (iii) The heat loss from pipes and equipment is negligible, and the flue gas heat carrier is non-condensable and non-corrosive during the heat transfer process.

Fig. 4 shows the T-s diagram of the ORC-based heat recovery system. The shape of the saturation curves correspond to R245fa working fluid and has been generated using the EES software [16]. A thermodynamic model is developed. The energy balance equations and the performance indicators are presented in Appendix A.

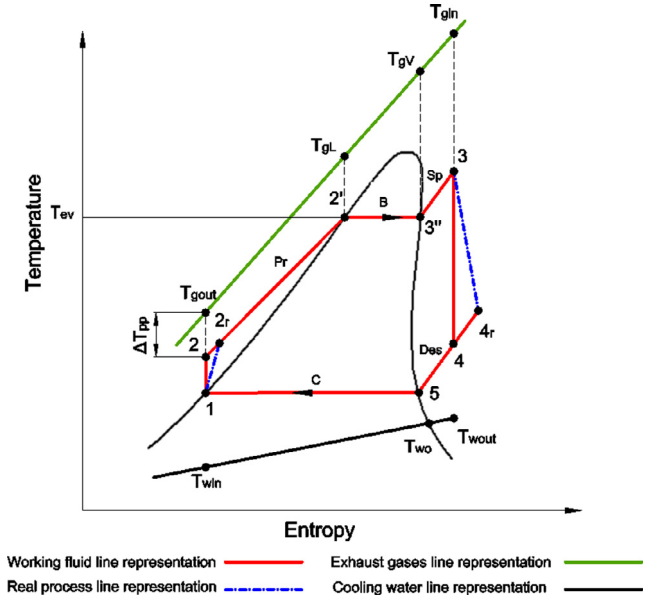

Fig. 4. T-s diagram of the ORC system.

4.1. Heat transfer model

4.1.1. Phase transition zones

The evaporator is conceptually divided into three zones, namely a preheater, a boiler and a superheater, respectively, linked in series. These zones are associated with the phase transitions of the working fluid (Fig. 5). Though the evaporator surface is fixed, the surface area of the three zones is changing, depending on the operation regime. Determination of the three surface areas, A_{pr}, A_b and A_{sp}, respectively, is one of the objectives of the present model.

4.1.2. Fluid properties

4.1.2.1. Properties of flue gas. The properties of flue gas can be calculated by using the EES software [16]. The main components in the flue gas of Diesel engines are CO_2, H_2O, N_2, and O_2. Moreover, the mass fractions of these components vary with the ICE operating regime. Here the following mass fractions of components for flue gas is adopted [17]: $g_{CO2} = 0.091$, $g_{H2O} = 0.074$, $g_{O2} = 0.093$, $g_{N2} = 0.742$.

For evaporator zones, the specific heat, dynamic viscosity, conductivity and Prandtl number of the flue gases depend on the gases temperature at each zone. For example, in the evaporator zone, the temperature of gases ranges between the outlet temperature of flue gas (T_{gout}) and the inlet temperature of flue gas (T_{gin}). Therefore, the average temperature of flue gas in the evaporator (T_{tot}) is given by:

$$T_{tot} = \frac{T_{gin} + T_{gout}}{2} \quad (1)$$

Similarly, in the preheater zone, the bulk temperature of flue gases (T_{pr}) is given by:

$$T_{pr} = \frac{T_{gout} + T_{gL}}{2} \quad (2)$$

and the bulk temperature of the flue gases in the boiler zone (T_b) is given by:

$$T_b = \frac{T_{gL} + T_{gV}}{2} \quad (3)$$

4.1.2.2. Properties of cooling water. For the two zones of the condenser, the specific heat, dynamic viscosity, conductivity and Prandtl number of the cooling water depends on the water temper-

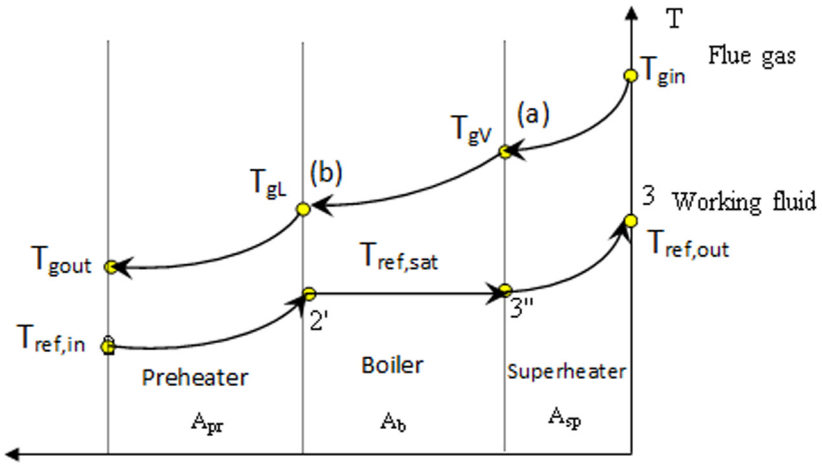

Fig. 5. The three zones of the evaporator (preheater, boiler, superheater).

ature at each zone. For example, in the desuperheater zone, the cooling water temperature ranges between the temperature of water outlet (T_{wout}) and the temperature of cooling water inlet, T_{wo}. So, the bulk temperature of cooling water (T_{des}) is given by:

$$T_{des} = \frac{T_{wout} + T_{wo}}{2} \tag{4}$$

For the condensation zone, the bulk temperature of cooling water (T_{con}) is given by:

$$T_{con} = \frac{T_{win} + T_{wo}}{2} \tag{5}$$

4.2. Logarithmic-mean temperature difference method (LMTD)

The logarithmic mean temperature difference (LMTD) method is often used during heat exchanger analysis [18,19]. The LMTD is defined as:

$$\Delta T_m = \frac{\Delta T_{max} - \Delta T_{min}}{\ln\left(\frac{\Delta T_{max}}{\Delta T_{min}}\right)} \tag{6}$$

where ΔT_{max} is the maximum temperature between the two fluids at each end of the heat exchanger, and ΔT_{min} is the minimum temperature between the two fluids.

4.3. Overall heat transfer coefficients and zone surface areas

Details about the overall heat transfer coefficients and zone surface areas are given in Appendix B.

4.4. Heat fluxes and heat recovery efficiency

The following equations can be used to determine the heat fluxes rejected from the condenser and the heat fluxes released from the desuperheater and condensation zones, respectively:

$$\dot{Q}_{rej} = \dot{m}_w C_w (T_{wout} - T_{win}) \tag{7}$$

$$\dot{Q}_{des} = \dot{m}_{ref}(h_{4r} - h_5) \tag{8}$$

$$\dot{Q}_{condensation} = \dot{m}_{ref}(h_5 - h_1) \tag{9}$$

Note that:

$$\dot{Q}_{rej} = \dot{Q}_{des} + \dot{Q}_{condensation} \tag{10}$$

The heat available in the flue gas can be only partially recovered using the ORC technology. An efficiency indicator for the heat recovery process, which actually takes place in the evaporator, has been proposed in [20]. The heat recovery efficiency (η_r) is defined by the ratio of the heat flux absorbed by the working fluid from the flue gas, and the maximum heat flux which can be recovered from the flue gas, $\dot{Q}_{max}$ [20]:

$$\eta_r = \frac{\dot{Q}_{gases}}{\dot{Q}_{max}} \tag{11}$$

where $\dot{Q}_{max}$ is given by:

$$\dot{Q}_{max} = \dot{m}_g C_{p,g}[T_{gin} - (T_2 + \Delta T_{amb})] \tag{12}$$

In Eq. (12) $\dot{m}_g$ is the mass flow rate of the flue gas, $C_{p,g}$ is the specific heat at constant pressure of the flue gas and the term $T_2 + \Delta T_{amb}$ stands for the minimum theoretical value of the flue gas temperature at the exit of the evaporator, which can be achieved for a given application.

4.5. Model implementation and validation

The model is implemented under the EES environment. Most previous studies validated the models by comparison with results by others authors, which, in turn, were obtained by simulation [3,9,11]. Therefore, this sort of validation is in fact a model intercomparison. The same procedure is used here. Comparison with results reported in [19] (obtained by simulation, using measured data input) are performed. The input data used here are [21]: t_{ev} = 131.5 °C, p_{ev} = 24 bar, increment of superheating = 35 °C.

Fig. 6 shows good agreement between results obtained by using the present model and results reported in [21]. The heat flux transferred in preheated and boiler in the present work is slightly higher than that of [21], while the heat flux received in the superheater in [21] is slightly higher than that of the present work (Fig. 6a). Fig. 6b shows that the ratio of preheated area in the present work is very close to that of [21] while the present ratio of boiler area is slightly higher than that of [21], similarly with the working fluid mass flow rate (Fig. 6c) and the temperature of the gas at the medium points (a), (b) presented in Fig. 5 (Fig. 6d). The ratio of superheater area in [21] is slightly higher than that of the present work (Fig. 6b).

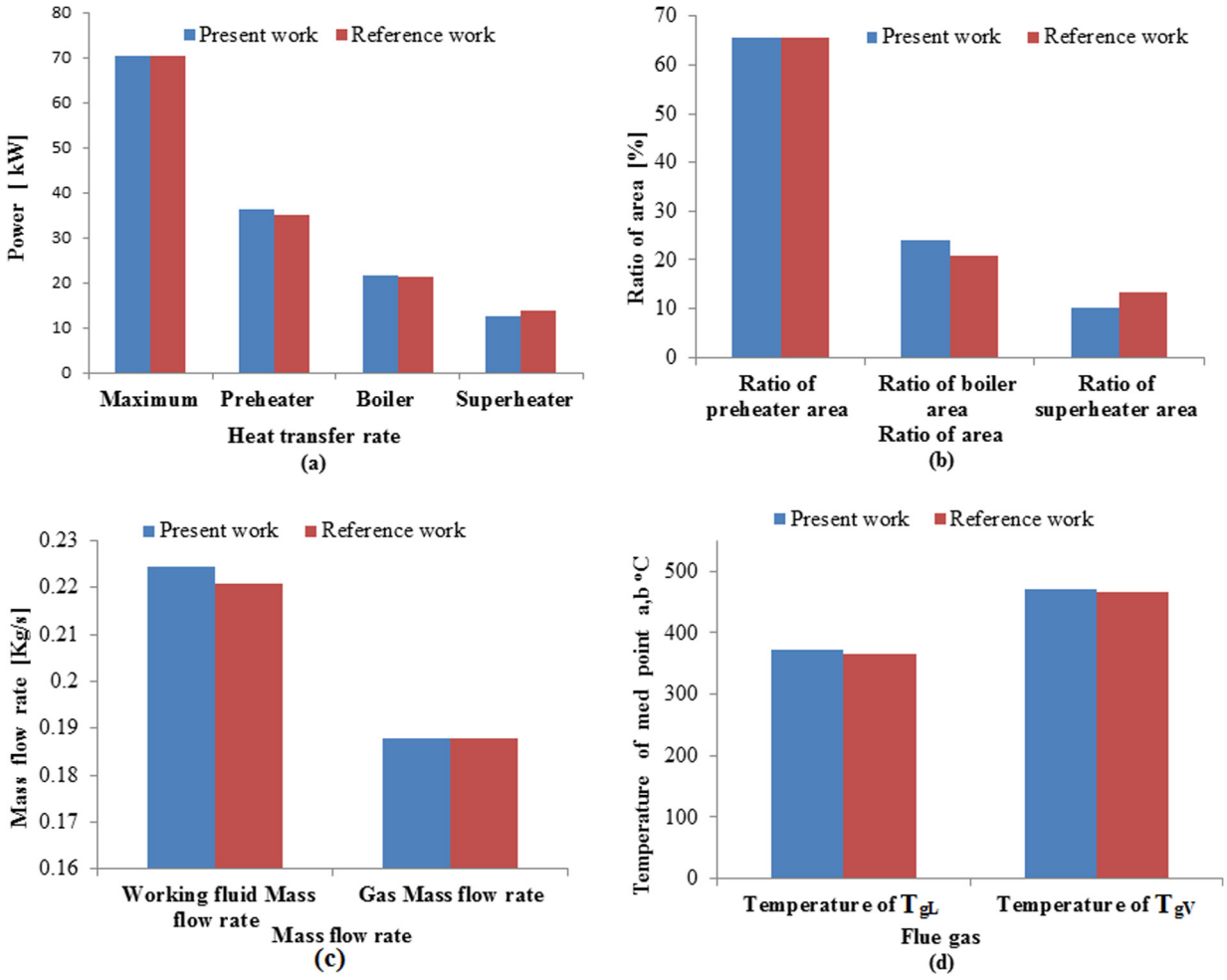

Fig. 6. Comparison between results obtained in present work and reference study [21].

5. Results

In Section 5.1 the performance of ORC-based systems for different operation regimes is treated. Based on these results, an original method is proposed in Section 5.2 for the design of ORC-based systems for the recovery of waste heat by internal combustion engines, used to driving electric generators. As a novelty, the design method covers the optimum operation of ORC-based systems coupled with partially loaded EGs. The method consists of finding the optimum evaporator pressure and designing the geometry of the evaporator and condenser associated with the maximum net power. A procedure based on the continuous optimization of the working fluid mass flow rate is also proposed for the operation of the ORC-based system.

Table 2
Main input data.

Parameter	Specification	Value	Units
Ambient temperature	t_{amb}	20	°C
Inlet water temperature of cooling system	t_{win}	20	°C
Outlet water temperature of cooling system	t_{wout}	30	°C
Pump efficiency	η_P	0.8	—
Expander efficiency	η_{exp}	0.7	—
Inside diameter of inner heat exchanger tube	d_i	0.03	m
Outside diameter of inner heat exchanger tube	d_o	0.04	m
Outside diameter of outer heat exchanger tube	D	0.06	m

Table 2 shows input data used in present analysis. These data are kept unchanged except for the values of the flue gas temperature and flue gas mass flow rate.

The results obtained in the paper apply for isentropic fluids. Note that when dry fluids are used the configuration of the ORC-based system is different from that of Fig. 3. First, the superheater is not needed when dry fluids are used. Second, the ORC-based system must be equipped with a counter-current heat exchanger (gas to liquid), which is placed between the outlet of the expander and the inlet of the condenser (on the hot side) and between the output of the pump and the inlet of the evaporator (on the cold side). The reason is that the fluid has not reached the two-phase state at the end of the expansion; its temperature at this point is higher than the condensing temperature. This higher temperature fluid can be used to preheat the liquid before it enters the evaporator. The power required from the heat source is therefore reduced and the efficiency is increased.

5.1. Performance of ORC-based systems for different ORC operation regimes

The performance of the ORC-based systems depends significantly on the ORC operation regime. Fig. 7 shows that the surface area of the superheater increases and the boiler area decreases, by increasing the inlet expander temperature t_3. The preheater zone area increases by increasing t_3. For $t_3 = 120$ °C, the surface area of the superheater is about 4% of the area of the evaporator

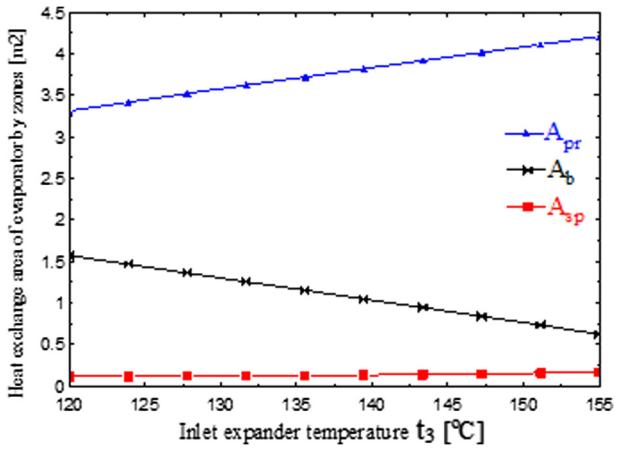

Fig. 7. Effect of inlet expander temperature on the area of evaporator zones at t_c = 27 °C; Superheating increment = 10 °C; EG load = 100%.

while for the boiler and preheater, the area is 30% and 66%, respectively. For t_3 = 150 °C, the surface area of the superheater is about 3% of the area of the evaporator while for the boiler and preheater the area is 15% and 82%, respectively.

Generally, the expander power increases by increasing the inlet expander temperature (Fig. 8). When the EG operates at partial load, the temperature of the flue gas decreases, as compared to the case of full load. As a consequence, the expander output power decreases.

When the EG load increases, the temperature and mass flow rate of flue gas are increasing. Also, the inlet expander temperature of the working fluid increases and the power of the expander increases, too (Fig. 8).

Most previous studies about the performance of the ORC systems coupled with ICE assumed that the engine is operating at full load. There are many practical applications when ICEs are operating at partial load. Examples are ICEs used in transportation [22] and small district heating systems [23]. Present results confirm that partial loaded EGs make the ICEs to operate at partial load and this has consequences on the performance of the ORC systems. This issue is analyzed in more details in Section 5.2.

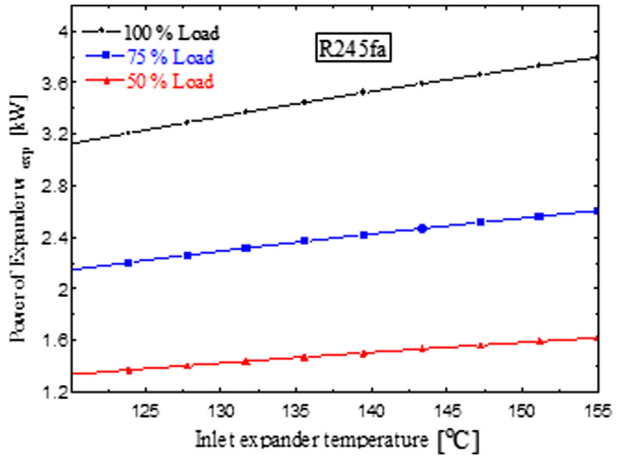

Fig. 8. Effect of the inlet expander temperature on the expander output power for different EG loads at t_c = 27 °C.

5.2. Optimum operation of ORC-based systems coupled with partially loaded EG

The model presented in Sections 4.1–4.4 contains the tools necessary to design and estimate the performance of ORC-based systems coupled with EGs operating at partial load. However, the model implementation is different from that of Section 4.5 and is described in Section 5.2.1. Section 5.2.2 shows results concerning the optimum evaporation pressure while Section 5.2.3 shows how the ORC-based systems are designed. Finally, the performance of the ORC-based system is evaluated in Section 5.2.4, by taking into account the partial load of the EG/ICE. Isentropic working fluids (R245fa, R123, R141b and R600a) [12,24,25] are used as examples.

5.2.1. Model implementation and validation

Table 3 shows the input (measured) data used in case of partial loaded EG/ICE.

The mass flow rate of the working fluid is optimized in order to maximize the net power and to ensure that the working fluid is superheated at the expander inlet. A code is developed under the EES environment.

The results obtained by using the present model are compared with results presented in [26,11], for similar operation conditions (see Table 4). The ORCs in [26,11] have been driven by ICE flue gas with temperature of 470 °C and mass flow rate of 0.53 kg/s. The condensation temperature t_c was 35 °C, the isentropic expander efficiency was 0.7, and the isentropic pump efficiency was 0.8. The evaporation pressure varied between the condensation pressure p_{con} and the critical pressure p_{cr}. Table 5 shows good agreement between results obtained here and in [26,11].

5.2.2. Optimum evaporator pressure

There is an optimum evaporation pressure for which the net power reaches the maximum value. Fig. 9 shows the dependence of the net power on the evaporation pressure, for different superheating increments, for R245fa. Results correspond to full EG load (100%), which means that the heat flux driving the evaporator is 20.24 kW [27]. The optimum evaporation pressure, as well as the maximum net power, depends on the superheating increment. The maximum net power corresponds to a superheating increment of 30 °C.

Other working fluids, such as R600a, R123 and R141b shows, generally, features which are similar with those of R245fa. However, the shape of the curve describing the locus of the maximum net power depends on the working fluid.

5.2.3. ORC system design

The optimum value of the evaporation pressure is used as input when the ORC system is designed. The design involves three steps: (1) computing the geometry of the ORC-based system (Section 5.2.3.1); (2) evaluation of working fluid mass flow rate as a function of the variable incoming heat flux in the evaporator, due to partial loaded EG/ICE (Section 5.2.3.2) and (3) performance estimation for partial loaded EG/ICE (Section 5.2.3.3).

Table 3
Input (measured) data for partial loaded electric generator.

Parameter	Symbol	Value	Units
Flue gas mass flow rate (100% Load)	$\dot{m}_g$	0.053	kg/s
(75% Load)		0.0494	kg/s
(50% Load)		0.0475	kg/s
Flue gas temperature (100% Load)	$t_{g,in}$	477	°C
(75% Load)		403	°C
(50% Load)		327	°C

Table 4
Comparison between results obtained in this work and in [26,11].

Working fluid	ORC net power, P_{net} (kW)	ORC thermal efficiency, η_{th} (%)	Condensation pressure, p_{con} (kPa)	Evaporation pressure, p_{ev} (kPa)	Evaporation temperature, T_{ev} (K)	Working fluid mass flow rate, $\dot{m}_{ref}$ (kg/s)	Specific volumes ratio, $\upsilon 4/\upsilon 3$	ORC specific work output, $\Delta h_{3\text{-}4}$ (kJ/kg)	Reference
R11	273.7	15.90	14.72	3835.9	461.5	7.475	31.95	42.2	27
R11	290.3	16.58	14.79	3835.9	461.0	7.487	32.00	41.9	26
R11	274.9	15.97	14.79	3835.0	461.5	7.390	28.07	42.7	This work
R134a	145.9	8.47	883.8	3723.4	369.9	9.000	5.3	19.2	27
R134a	147.5	8.52	883.3	3723.4	369.9	8.966	5.0	19.4	26
R134a	147.1	8.54	887.5	3723.0	369.9	8.814	4.9	19.7	This work

Table 5
Four operation cases for the ORC-based system. All working fluids are isentropic.

Operation case	Working Fluid	Optimum evaporation pressure p_{opt}, bar	Evaporation temperature t_{ev}, °C	Minimum pinch point temperature difference ΔT_{gpp}, °C	Heat flux absorbed in the evaporator Q_{source} kW	ORC net power P_{net}, kW	ORC thermal efficiency η_{th}, %	Inlet temperature of flue gas t_{gin}, °C	Outlet temperature of flue gas t_{gout}, °C	Working fluid mass flow rate $\dot{m}_{ref}$, kg/s	Environmental effects	Suitability Yes or no
1	R245fa	33.37	149.3	102.2	20.24	2.457	12.1	477	140.3	0.0659	Very good	Yes
2	R141b	36	193.9	103.9	20.24	3.361	16.6	477	140.3	0.05613	bad	No
3	R123	36	182.5	101.2	20.24	3.198	15.8	477	140.3	0.07274	good	Yes
4	R600a	34.71	130.6	101.4	20.24	2.112	10.4	477	140.3	0.04086	bad	No

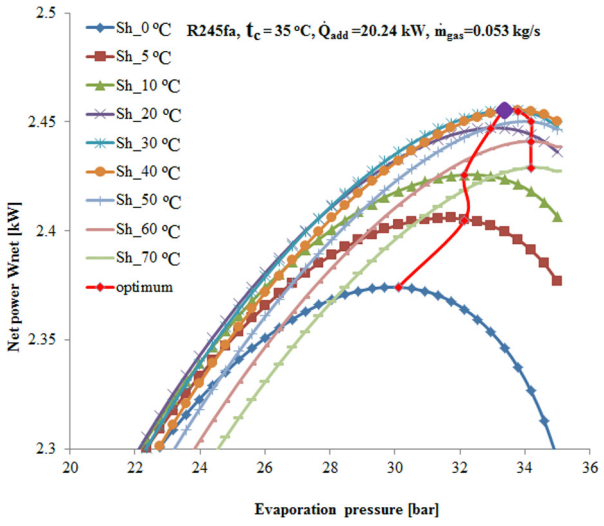

Fig. 9. Effect of evaporation pressure on net power for different superheating increments for R245fa.

5.2.3.1. Geometry of ORC-based system. Essentially, computing the geometry of the ORC-based system means to determining the surface areas and tube lengths of the evaporator and condenser. Four ORC operation regimes are considered, as follows: (1) R245fa with a superheating increment of 30 °C; (2) R141b with a superheating increment of 40 °C; (3) R123 with a superheating increment of 30 °C; (4) R600a with a superheating increment of 30 °C (see Table 5).

The model presented in Section 4 is used to analyze the four operation regimes of Table 5. Table 6 shows the results obtained for the total surface area of evaporator and condenser, as well as the surface area of the preheater, boiler, supereheater, desuperheater and condensation zones, respectively. Also, the lengths of the tubular evaporator and condenser are shown.

The smallest values for the evaporator area are obtained for operation cases #4 and #1 while the highest ones correspond to operation cases #2 and #3. Regarding the condenser, the smallest values of its area are obtained for operation cases #4 and #2 while the highest ones are associated with operation cases #3 and #1. The smallest evaporator length is obtained for operation cases #4 and #1, while the highest ones for operation cases #2 and #3. The condenser lengths are comparable, for all operation cases. When the evaporator is considered, for each operation case, the preheater area has the highest value, while the area of the boiler can be smaller or higher than the one of the superheater, depending on the operation case. In case of the condenser, the area of the desuperheater is always smaller than the area of the condensation zone, as expected.

The optimized cycle configuration is determined for four cases of Table 5. For each case the condensing temperature is considered to be 35 °C. This leads to the following condensation pressures: case #1 2.1 bar, #2 1.1 bar, #3 1.3 bar and #4 4.6 bar, respectively. This means that at the condenser level there is no risk of air ingress and the technical problem of expensive sealing has been overcome.

5.2.3.2. Working fluid mass flow rate for variable heat absorbed in the evaporator. The following two parameters related to the (output) performance of the ORC are sensitive to the heat absorbed in the

Table 6
Surface areas and lengths of the tubular evaporator and condenser for the operation cases of Table 5.

Operation case	Evaporator area, A_{evap} (m^2)	Preheater area (m^2)	Boiler area (m^2)	Superheater area (m^2)	Condenser area, A_{con} (m^2)	Desuperheater area (m^2)	Condensation area (m^2)	Evaporator length, L_{ev} (m)	Condenser length, L_{con} (m)
1	2.189	1.687	0.2365	0.2657	2.458	0.3319	2.126	17.6	19.57
2	2.731	2.039	0.3653	0.3271	2.444	0.2689	2.175	21.75	19.46
3	2.406	1.973	0.1347	0.2979	2.513	0.2969	2.216	19.15	20
4	2.03	1.544	0.1014	0.3848	2.417	0.3762	2.095	16.16	19.67

evaporator: the expander output power and the net output power, respectively. Both parameters may be maximized by optimizing the working fluid mass flow rate. By optimizing the working fluid mass flow rate, the expander output power is maximized firstly. Secondly the maximized value of the net output power is computed by subtracting from the maximized expander output power the power of the pump, which has a certain computed value. Therefore, the two outputs are not independent of each other.

First, the expander output power is considered.

At this stage the geometry of the evaporator and condenser is designed as shown in Section 5.2.3.1. Assume, in addition, that the mass flow rates of the ORC working fluid and coolant fluid in the condenser are fixed. Then, changing the heat flux absorbed in the evaporator makes the state 3 in all subfigures of Fig. 10 to move. Depending on the amount of incoming heat, the state 3 may belong to the superheated region or to the wet vapor region. However, proper expander operation requires the state 3 be placed in the superheated region, for any value of the incoming heat flux. Since the geometry is fixed, this may be ensured by an appropriate change of the working fluid mass flow rate. The design objective is to find that specific optimum working fluid mass flow rate which maximizes the expander output power.

As an example, an ORC-based system (using R245fa as working fluid) coupled with an EG/ICE operating at full or partial load is considered. The variable ICE load is associated with variable flue gas temperature entering the evaporator, $t_{g,in}$, and with variable heat flux transferred to the evaporator, Q_{tot}. Fig. 10a–e shows the results. When the EG/ICE load changes, the temperature of flue gas changes. Therefore, the position of state 3 moves when the EG/ICE load is changing, as expected. Also, the optimum mass flow rate of the working fluid is changing.

Next, the net output power is considered.

The dependence of the net power on the mass flow rate of the isentropic working fluid R245fa at full and partial load of the EG/ICE is shown in Fig. 11a–c. The maximum net power decreases by decreasing the percentage of the EG load since the temperature of the flue gas decreases in this case. The optimum mass flow rate decreases, too.

5.2.3.3. Performance estimation for partial loaded EG. Partial loaded EGs make the ICE to operate at partial load. Changing the mass flow rate at partial ICE load is associated with changes of other quantities.

The power consumed by the pump increases by increasing the working fluid mass flow rate (Fig. 12). The power generated by the expander has a maximum in respect with the mass flow rate. Similarly, the net power is a maximum, corresponding to the optimum mass flow rate. For the particular case of Fig. 12, the optimum mass flow rates that lead to a maximum net output power for the working fluid R245fa are as follows: 0.06327 kg/s, 0.04653 kg/s and 0.03204 kg/s for 100% EG load, 75% EG load and 50% EG load, respectively. Also, in Fig. 12 one can see that the mass

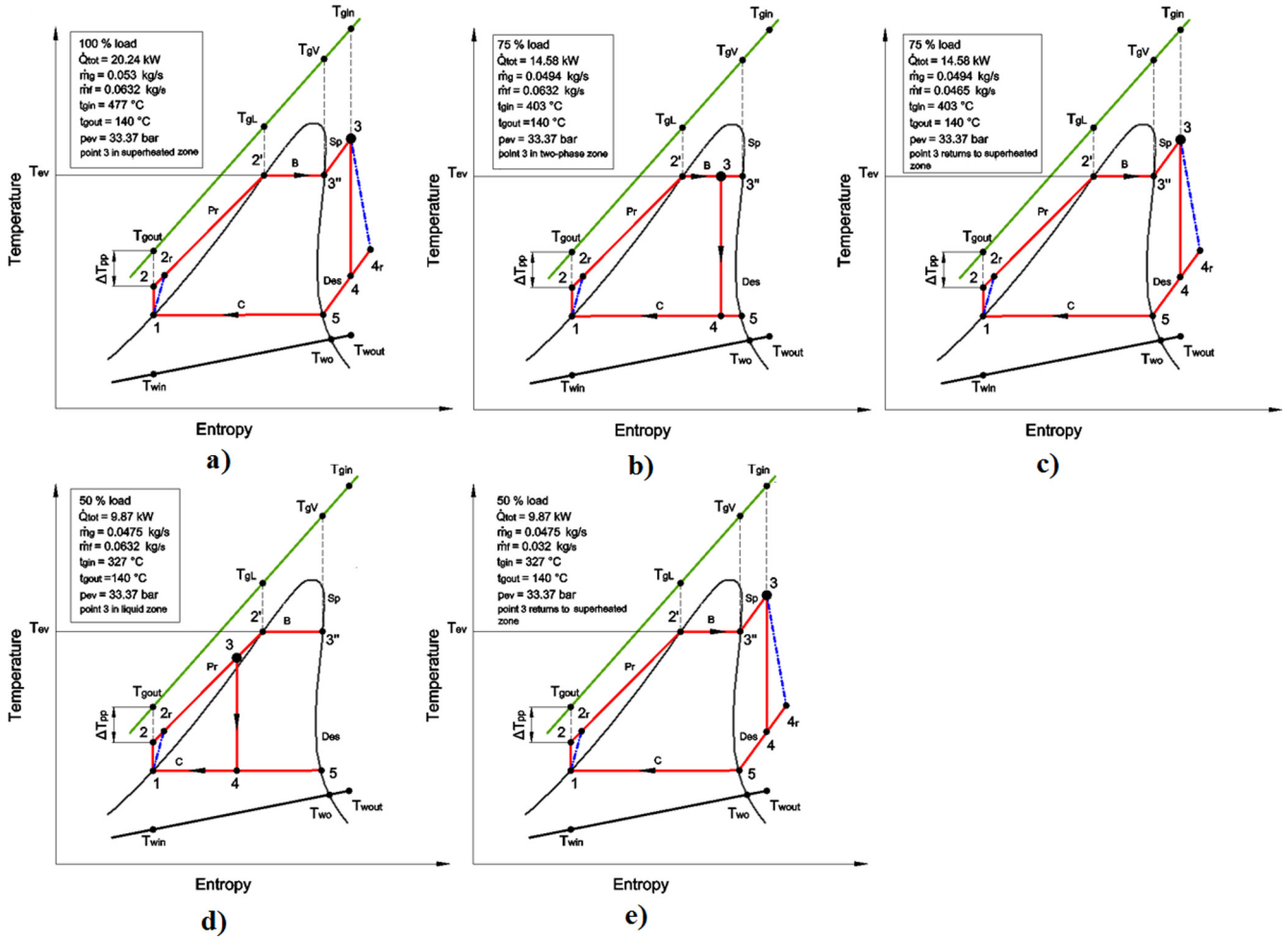

Fig. 10. T-s diagram for R245fa, for different EG/ICE loads. (a) 100% EG/ICE load; (b) same as (a) but 75% EG/ICE load; (c) same as (b) but optimum working fluid mass flow rate; (d) 50% EG/ICE load, same working fluid mass flow rate as in (a); (e) same as (d) but optimum working fluid mass flow rate is considered.

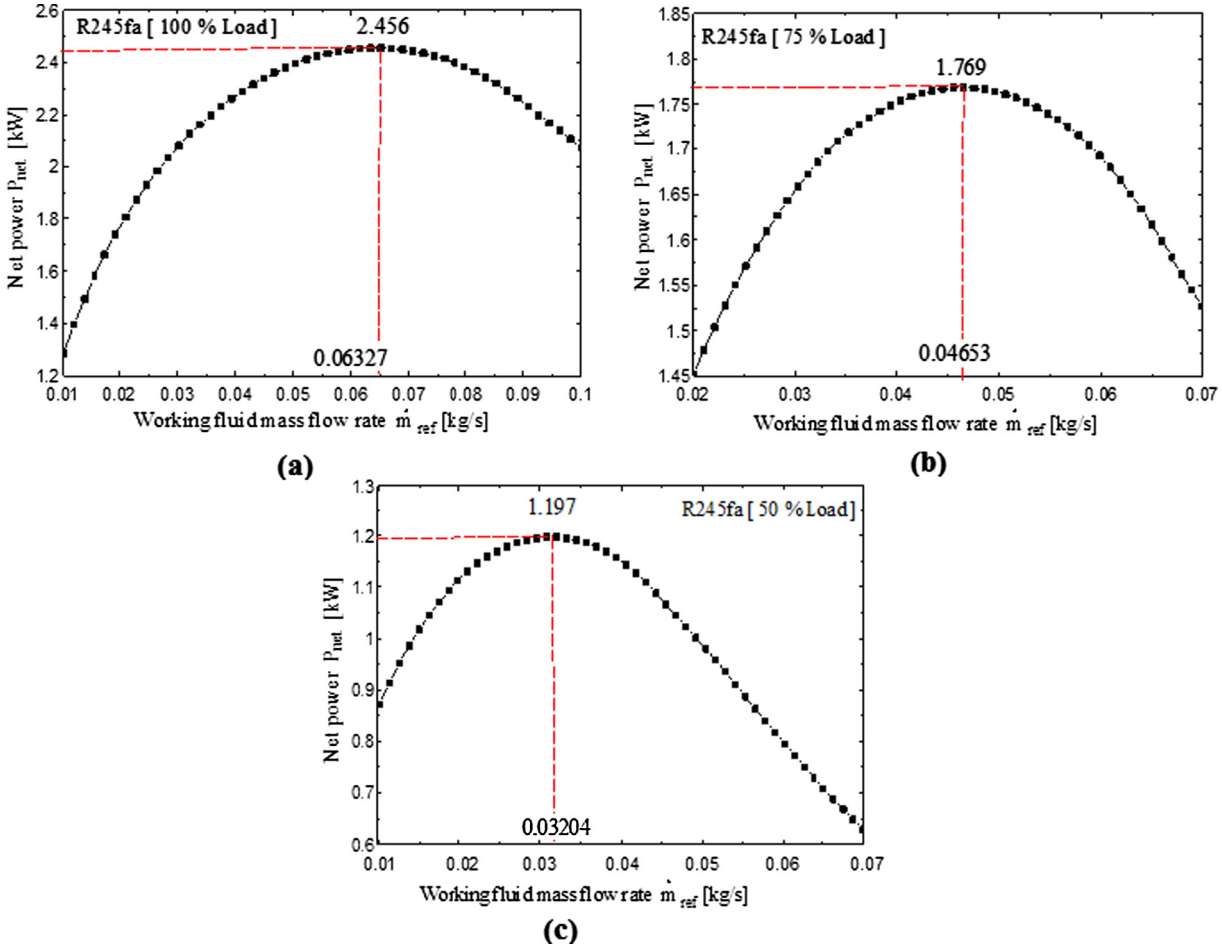

Fig. 11. Effect of working fluid mass flow rate on net power for R245fa at different EG loads. (a) 100% EG load; (b) 75% EG load; (c) 50% EG load.

flow rate values corresponding to the maximum power generated by the expander are higher than the ones that correspond to the maximum net power.

The total heat flux generated in the ICE by fuel combustion is given by [28]:

$$P_{tot} = \dot{m}_{fuel} LHV \tag{13}$$

where LHV denotes the lower heating value of the fuel. The thermal efficiency of the ICE is calculated by:

$$\eta_{ICE} = \frac{P_{ICE}}{P_{tot}} \tag{14}$$

where P_{ICE} is the ICE power. The thermal efficiency of the ICE combined with the ORC-based system may be computed by:

$$\eta_{ICE-ORC} = \frac{P_{ICE-ORC}}{P_{tot}} = \frac{P_{ICE} + P_{net}}{P_{tot}} \tag{15}$$

Table 7 shows the effect of EG load variation on the ORC-based system performance. A few comments follow:

- The ICE flue gas temperature and ICE flue gas mass flow rate decrease when the EG load decrease;
- The optimum working fluid mass flow rate for the ORC-based systems decreases by decreasing the EG load, for the same value of the superheating increment;
- In case of the working fluid R245fa, the evaporating pressure 33.3 bar and the expander inlet turbine temperature 179 °C lead to maximum net output power of the ORC-based system;
- The heat flux absorbed in the evaporator decreases by decreasing the EG load, which furthermore leads to lower maximum output power and lower thermal efficiency for the ORC- based system;
- Assuming the same lower heating value (LHV) of fuel, lower EG loads lead to lower net power, lower fuel mass flow rate and lower thermal efficiency of the ICE;
- The thermal efficiency of the combination ICE-ORC-based system decreases as the EG load decreases.
- The thermal efficiency of the combination ICE – ORC-based system increases with respect to the efficiency of the ICE operating alone as follows: 6.00%, 5.85% and 5.91%, for the EG loads of 100%, 75% and 50%, respectively.

The design method proposed in this paper delivers design data for a simple ORC configuration in case of waste heat recovery for an EG operating at full load. The design data mainly involves optimum operation pressures, temperatures, superheating degree, working fluid mass flow rate and geometry of the heat exchangers that lead to maximum net output power for a given working fluid (R245fa, for instance). After designing the ORC system an analysis is carried out in terms of variable EG loads, meaning variable heat inputs. This means that the ORC system is build involving fixed heat exchanger geometry, fixed pump and expander configurations.

The results show that, for isentropic working fluids, there is an optimum evaporation pressure and superheating degree that give an optimum expander inlet temperature (point 3 in Fig. 10) for

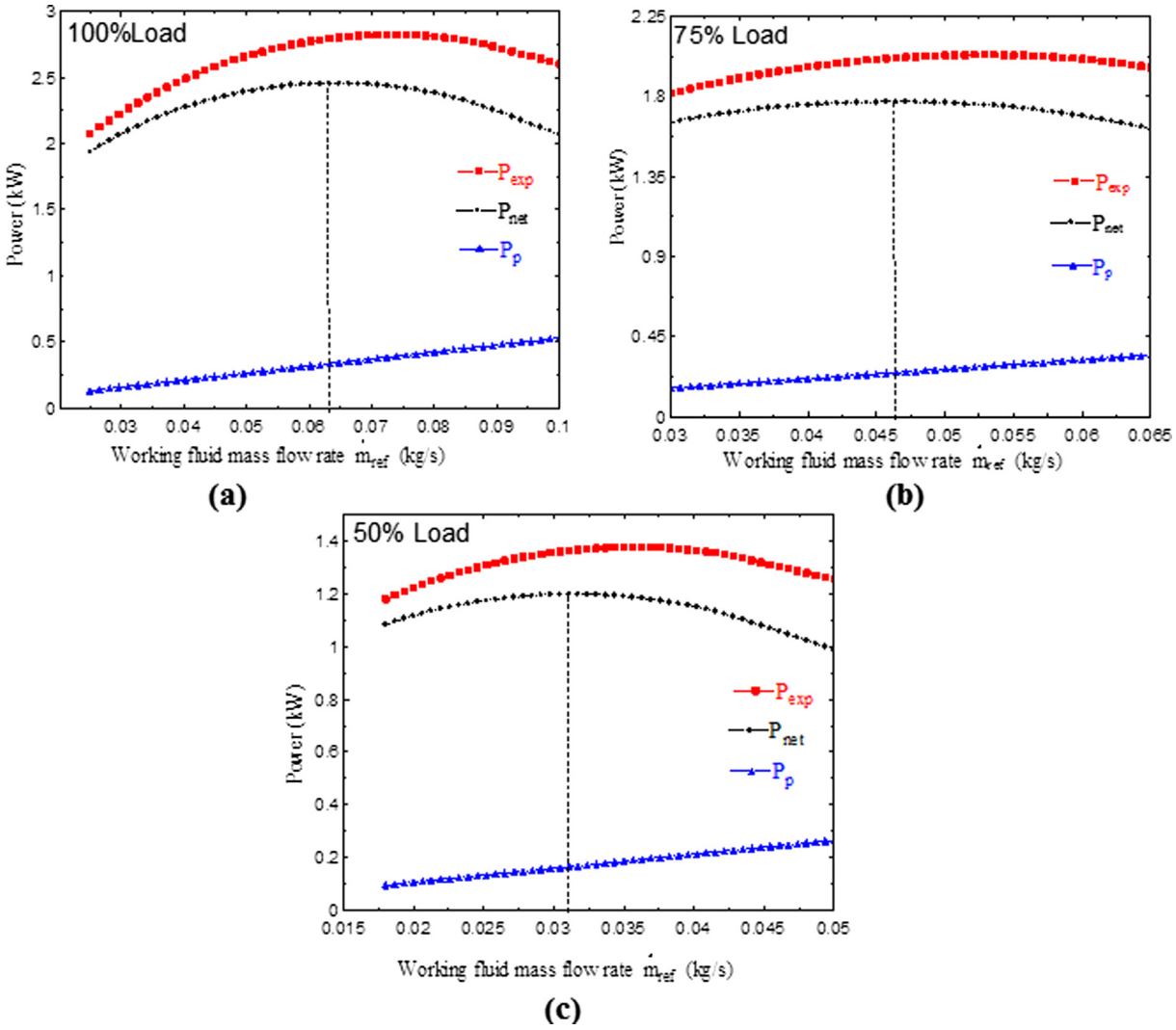

Fig. 12. Expander power, net power and pump power for R245fa at different EG loads. (a) 100% EG load; (b) 75% EG load; (c) 50% EG load.

Table 7
Effect of EG load variations on ORC-based system performance (working fluid: R245fa).

Parameter	Symbol	Units	100%	75%	50%
ICE flue gas temperature	t_{gin}	°C	477	407	327
ICE flue gas mass flow rate	$\dot{m}_g$	kg/s	0.053	0.049	0.047
Optimum working fluid mass flow rate	$\dot{m}_{ref}$	kg/s	0.06327	0.04653	0.03204
Superheating increment	ΔT_{sup}	°C	30	30	30
Evaporation pressure	P_{ev}	bar	33.3	33.3	33.3
Inlet expander temperature	t_3	°C	179	179	179
Heat flux absorbed in the evaporator	Q_{source}	kW	20.24	14.58	9.87
Maximum net power	P_{net}	kW	2.456	1.769	1.197
Thermal efficiency of ORC-based system	η_{th}	%	12.13	12.13	12.13
Lower heating value of fuel	LHV	kJ/kg	43,000	43,000	43,000
Net ICE power	P_{ICE}	kW	37.70	28.27	18.85
Fuel mass flow rate	$\dot{m}_{fuel}$	kg/s	0.0021	0.0017	0.0013
Thermal efficiency of the ICE	η_{ICE}	%	40.4	38.6	33.4
Thermal efficiency of the combination ICE-ORC-based system	$\eta_{ICE\text{-}ORC}$	%	43.0	41.0	35.5
Increase of thermal efficiency	$1-\frac{\eta_{ICE}}{\eta_{ICE-ORC}}$	%	6.00	5.85	5.91

an optimum working fluid mass flow rate that lead to maximum net output power.

For a fixed configuration of the ORC system, and for optimum evaporation pressure, when the EG is operating at partial load and the mass flow rate is kept constant, the point 3 in Fig. 10 (corresponding to the expander inlet) is moving towards the dry saturated curve. This means that the operation of the ORC system is not in the optimum point and there is a risk for the working fluid to enter the expander being in liquid phase. To avoid this, variable speed pumps can be used to continuously adjust the value of the

mass flow rate and keep the parameters of point 3 (mainly the temperature and superheating degree) constant, leading (for each value of the EG load) to optimum operation conditions (i.e. maximum net output power).

In this context the operational procedure outlined in this paper has as an objective the maximum net output power for each value of the EG load. This objective can be reached by adjusting the temperature of the working fluid in point 3 of Fig. 10 (expander inlet) to match the optimum superheating degree for the given fluid. The optimum superheating degree can be changed to match the required value by continuously changing the working fluid mass flow rate.

6. Conclusions

This paper refers to a topic which is not very often treated in literature, namely recovering waste heat from the hot gases exhausted by internal combustion engines (ICEs) driving electric generators (EGs) a partial load. The topic is of particular interest for developing countries where electric grids are underdeveloped or even missing and electricity is generated locally by using classical fuels. The heat recovery system treated here is based on Organic Rankine Cycles (ORCs). Isentropic working fluids are considered. A novel optimum design method is proposed for the ORCs coupled with EGs operating at partial loads. Several conclusions are emphasized next.

First, ORC-based systems coupled with ICEs operating at full EG load are considered. A steady state model for waste heat recovery based on energy balance equations is developed. The model is tested against results reported in literature and good agreement is found.

More specific results for operation at full EG load are as follows:

1. The maximum net output power for the particular cases studied here is obtained for R141b (3.361 kW), followed by R123 (3.198 kW), R245fa (2.454 kW) and R600a (2.112 kW).
2. The optimum superheating increment ranges between 30 and 40 °C, depending on the type of working fluids.
3. A pinch point temperature difference (ΔT_{out}) exits in the evaporator between the flue gas temperature and the working fluid at the evaporator inlet.
4. The total area of the evaporator is very close to the total area of the condenser, a fact which facilitates manufacturing.
5. The surface area of the preheater zone is about 75% of the total surface area, while those of the boiler zone and superheater zone are about 13.5% and 11.5%, respectively.

Second, the case of the ORC-based systems coupled with ICEs operating at partial EG load is studied. The model is used in the case of ORC-based systems driven by variable incoming heat flux at the evaporator. Comparison with results reported in literature shows good agreement.

The novel method for the optimum design of ORC-based systems operating in combination with ICE at partial EG loads starts by determining the optimum evaporator pressure. Next, the geometry of the evaporator and condenser is determined. Finally, the operation of the ORC-based system in combination with ICE operating at partial EG load is considered. The solution is to optimize the working fluid mass flow rate in order to obtain the maximum net power. Once the ORC-based system is properly designed, its performance, as well as the performance of the combination ICE – ORC-based system, may be evaluated.

More specific results for operation at partial EG loads are as follows:

6. The net output power may be maximized by optimizing the working fluid mass flow rate. The optimum mass flow rate changes when the EG is partially loaded. As an example, for the case treated here, the optimum values are 0.06327 kg/s, 0.04653 kg/s and 0.03204 kg/s for the EG loads of 100%, 75% and 50%, respectively.
7. When the ICE is coupled with an ORC-based system, the overall thermal efficiency of the combined system, $\eta_{ICE\text{-}ORC}$, is higher than the thermal efficiency η_{ICE} of the ICE operating alone. As an example, for the case treated here, $\eta_{ICE\text{-}ORC}$ is higher than η_{ICE}, by 6.00%, 5.85% and 5.91%, for the EG loads of 100%, 75% and 50%, respectively.

Acknowledgments

The authors gratefully acknowledge the support provided by Executive Agency for Higher Education, Research, Development and Innovation Funding of Romania [PN-II-PT PCCA-2011-3.2-0059, Grant No.: 75/2012]. One author (MHKA) thanks the Ministry of Higher Education of Iraq for financial support during the preparation of this work. The authors thank the reviewers for useful comments and suggestions. The comments by one of the reviewers concerning waste heat recovery by using ORC applications in Europe and usage of dry working fluids are particularly welcome.

Appendix A.

A.1. Energy balance equations and performance indicators

A.1.1. Process 1–2 (across pump)

The working fluid leaves the condenser as saturated liquid and then it is pumped from state (1) to state (2) through an isentropic ideal process, while to state (2r) actually (Fig. 4). The power consumed by the pump can be expressed as [29,30]:

$$P_{P,actual} = \frac{P_{P,\ ideal}}{\eta_P} = \frac{\dot{m}_{ref}(h_1 - h_2)}{\eta_P} = \dot{m}_{ref}(h_1 - h_{2r}) \quad (A1)$$

where $P_{p,ideal}$ is the ideal power consumed by the pump, $\dot{m}_{ref}$ is the working fluid mass flow rate, η_p is the isentropic efficiency of the pump, h_1 is the enthalpy of the working fluid at the inlet and h_{2s} and h_{2r} are the isentropic and actual enthalpies of the working fluid at the outlet of the pump, respectively, for the ideal case. Enthalpy at state (1) is determined depending on two properties (as an example, as a function of the temperature and pressure at state 1).

The procedure to estimate the working fluid properties is as follows. In each state, knowing the values of two properties is necessary. They are used as input to obtain the values of other properties, in the same state. The Engineering Equation Solver (EES) [16] is used here for this purpose. The pressure of state 1 depends on the temperature and the quality of state 1. The quality of state 1 is zero because the fluid is saturated. In the same way, the specific entropy, specific volume, mass density and specific enthalpy at state 1 can be obtained. The process 1–2 is isentropic, meaning that the entropy at states 1 and 2 is the same. Now, one of the properties of state 2 is known, but one needs another property to obtain all of the properties of state 2. In the beginning, one estimates the evaporation pressure, to calculate the temperature, mass density, specific volume and specific enthalpy of state 2.

A.1.2. Process 2–3 (across evaporator)

The values of the evaporation pressure at states 2 and 3 are equal: $p_{ev} = p_2 = p_3$. The specific enthalpy of state 2r can be calculated as a function of pump efficiency, as follows:

$$h_{2r} = h_1 + \frac{h_2 - h_1}{\eta_P} \quad (A2)$$

Depending on the specific enthalpy and evaporation pressure at state 2r, the specific entropy and evaporation temperature (t_{ev}) can be obtained. Also, the inlet expander temperature (state 3) can be calculated as follows:

$$t_3 = t_{ev} + \Delta t_{sp} \quad (A3)$$

Here Δt_{sp} is the superheating increment over the evaporation temperature. Now the two parameters are known so, the specific entropy, specific volume, mass density and the specific enthalpy can be determined.

The process between states 3 and 4 is assumed to be isentropic. Thus, the entropy of state 3 is equal to the entropy of state 4. Now, the entropy and the pressure is known at state 4, because state 4 and state 1 have the same pressure (condensation pressure), and, based on these parameters, one can determine the temperature, specific volume, mass density and specific enthalpy in state 4. The specific enthalpy of state 4r can be calculated depending on expander efficiency, as follows:

$$h_{4r} = h_3 - \frac{h_3 - h_4}{\eta_{exp}} \quad (A4)$$

Now one has information about all the processes in the ORC, but information about the heat source is not known, except the inlet flue gas temperature to the evaporator, which ranges between 289 and 477 °C, depending on the EG load. In the first step, the ORC can be designed assuming full EG load (100%), where the flue gas temperature is 477 °C and the flue gas mass flow rate is 0.053 kg/s [14].

The procedure is as follows. First, a minimum pinch point temperature difference (ΔT_{pp}) between T_{gout} and T_2 to meet the gas heat exchanger performance is assumed to be 100 °C. Next, the minimum pinch point temperature difference is modified to keep the flue gas temperature at the evaporator outlet more than 140 °C. This minimum threshold is used to avoid the formation of sulphuric acid during gas flow due to the sulphur content of the flue gas.

The heat exchange between the working fluid and flue gas may be treated in two steps, as follows:

Step 1. Assume that the minimum pinch point temperature difference ΔT_{pp} occurs between state 2 and T_{gout}, which means $T_{gout} = T_2 + \Delta T_{pp}$. This allows writing the following relationship, which is coming from the energy balance associated with full evaporation and superheating of the working fluid:

$$\dot{m}_{ref} = \frac{\dot{m}_g Cp_{g1}(T_{gin} - T_{gout})}{(h_3 - h_2)} \quad (A5)$$

Here the specific heat C_{pg1} is calculated according to the flue gas composition, at the average temperature between T_{gout} and T_{gin}.

Step 2. Two other energy balance equations allow to determine the flue gas temperature at the superheater outlet (T_{gV}) and at the boiler outlet (T_{gL}), as follows:

$$T_{gL} = T_{gout} + \frac{\dot{m}_{ref}(h_{2'} - h_2)}{\dot{m}_g C_{P_{g2}}} \quad (A6)$$

$$T_{gV} = T_{gL} + \frac{\dot{m}_{ref}(h_{3''} - h_{2'})}{\dot{m}_g C_{P_{g3}}} \quad (A7)$$

Here the specific heats Cp_{g2} and Cp_{g3} are calculated at the average temperature between T_{gout} and T_{gL}, and between T_{gL} and T_{gV}, respectively.

Therefore, during the working fluid heating process 2–3, four temperature differences exist between the flue gas and the working fluid: $\Delta T_{in} = T_{gin} - T_3$, $\Delta T_v = T_{gV} - T_{ev}$, $\Delta T_L = T_{gL} - T_{ev}$ and $\Delta T_{out} = T_{gout} - T_2$, respectively. It can be seen that ΔT_{out} is the pinch point temperature difference since it is the smaller temperature difference among all four temperature differences.

A.1.3. Process 3–4 (across expander)

The working fluid energy is converted into useful mechanical work in expander. The expander power is given by:

$$P_{exp,actual} = P_{exp,ideal}\eta_{exp} = \dot{m}_{ref}(h_3 - h_4)\eta_{exp} = \dot{m}_{ref}(h_3 - h_{4r}) \quad (A8)$$

where $P_{exp,ideal}$ is the ideal power of the expander, η_{exp} the expander isentropic efficiency, and h_3 and h_{4r} are the actual specific enthalpies of the working fluid at the inlet and outlet of the expander, respectively.

The net ORC power P_n is calculated as:

$$P_n = P_{exp,actual} - P_{P,actual} \quad (A9)$$

The thermal efficiency is defined as the ratio between the net ORC power and the incoming heat flux:

$$\eta_{th} = \frac{P_n}{\dot{Q}_{source}} = \frac{P_{exp,actual} - P_{P,actual}}{\dot{Q}_{source}} \quad (A10)$$

A.1.4. Process 4–1 (across condenser)

During the working fluid cooling process 4–1, three temperature differences may be defined between the working fluid and the coolant: $\Delta T_{cin} = T_1 - T_{win}$, $\Delta T_{cm} = T_1 - T_{wo}$ and $\Delta T_{cout} = T_4 - T_{wout}$, respectively.

A.1.5. Overall ORC system

The following equations can be used to determine the heat flux for the evaporator, superheater, boiler and preheater zone, respectively.

$$\dot{Q}_{source} = \dot{m}_{ref}(h_3 - h_2) \quad (A11)$$

$$\dot{Q}_{sp} = \dot{m}_{ref}(h_3 - h_3) \quad (A12)$$

$$\dot{Q}_b = \dot{m}_{ref}(h_3 - h_2) \quad (A13)$$

$$\dot{Q}_{pr} = \dot{m}_{ref}(h_2 - h_2) \quad (A14)$$

Also:

$$\dot{Q}_{source} = \dot{Q}_{sp} + \dot{Q}_b + \dot{Q}_{pr} \quad (A15)$$

Summation of heat fluxes for all zones equates the total heat flux for the evaporator.

Appendix B.

B.1. Overall heat transfer coefficients and zone surface areas

B.1.1. Evaporator

In the evaporator, the working fluid R245fa flows in the inner tube while the flue gas flows in the outer tube. This applies for all the three zones of Fig. B1. Details follow about the computation of the overall heat transfer coefficients and zone surface areas.

B.1.1.1. Superheater zone. For the working fluid side in the superheater part, the Reynolds number can be calculated as follows:

$$Re_{ref,sp} = \frac{\dot{m}_{ref} d_i}{Ac_{ref}\mu_{ref,v}} \quad (B1)$$

where the cross section surface area is given by:

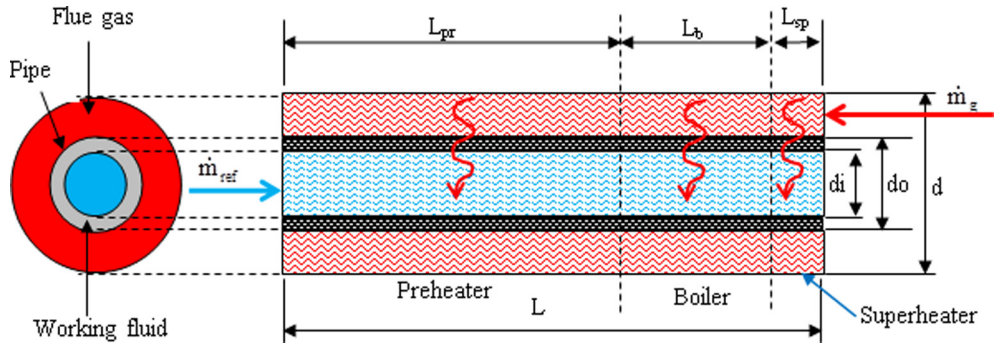

Fig. B1. Geometry of the Evaporator.

$$Ac_{ref} = \frac{\pi d_i^2}{4} \tag{B2}$$

If the flow is laminar ($Re < 2300$) and fully developed, the following equation may be used to find the heat transfer coefficient [31]:

$$H_{ref,sp} = 4.36\left(\frac{K_{ref,v}}{d_i}\right) \tag{B3}$$

If $0.5 \le Pr \le 2000$ and $3000 < Re < 5 \times 10^6$, the flow is turbulent and the Gnielinski equation may be used [32]:

$$H_{ref,sp} = \frac{\frac{f_{ref,sp}}{8}(Re_{ref,sp} - 1000)Pr_{ref,v}}{1.07 + 12.7\left(\frac{f_{ref,sp}}{8}\right)^{0.5}Pr_{ref,v}^{\frac{2}{3}} - 1}\left(\frac{K_{ref,v}}{d_i}\right) \tag{B4}$$

where

$$f_{ref,s} = \frac{1}{(0.79\ln(Re_{ref,sp}) - 1.64)^2} \tag{B5}$$

For the flue gas side, the Reynolds number is given by:

$$Re_{g,sp} = \frac{\dot{m}_g d_h}{Ac_g \mu_{g,sp}} \tag{B6}$$

where the equivalent diameter and the cross-section surface area are given by, respectively:

$$d_h = \frac{(d^2 - d_o^2)}{d_o} \tag{B7}$$

$$Ac_g = \frac{\pi d_h^2}{4} \tag{B8}$$

If the flow is laminar ($Re < 2300$) and fully developed, the heat transfer coefficient may be computed by:

$$H_{g,sp} = 4.36\left(\frac{K_{g,sp}}{d_h}\right) \tag{B9}$$

If $Re > 4000$ the flow is turbulent and the next relation may be used:

$$H_{g,sp} = \frac{\frac{f_{g,sp}}{8}(Re_{g,sp} - 1000)Pr_{g,sp}}{1.07 + 12.7\left(\frac{f_{g,sp}}{8}\right)^{0.5}Pr_{g,sp}^{\frac{2}{3}} - 1}\left(\frac{K_{g,sp}}{d_h}\right) \tag{B10}$$

where

$$f_{g,sp} = \frac{1}{(0.79\ln(Re_{g,sp}) - 1.64)^2} \tag{B11}$$

The overall heat transfer between gases and working fluid may be computed with:

$$U_{overall} = \frac{1}{\frac{1}{H_{ref}} + \frac{x}{k_t} + \frac{1}{H_g}} \cong \frac{1}{\frac{1}{H_{ref}} + \frac{1}{H_g}} = \frac{1}{\frac{H_{ref}+H_g}{H_{ref}\cdot H_g}} = \frac{H_{ref}\cdot H_g}{H_{ref} + H_g} \tag{B12}$$

The wall thickness (x) is very small and the wall conductivity (k_t) is high. Thus, we may assume $x/k_t \approx 0$.

Usage of Eq. (B12) gives the overall heat transfer coefficient U_{sp} in the superheater zone:

$$U_{sp} = \frac{H_{ref,sp}\cdot H_{g,sp}}{H_{ref,sp} + H_{g,sp}} \tag{B13}$$

Then, usage of the energy balance equation yields the surface area of the superheater zone:

$$A_{sp} = \frac{\dot{Q}_{sp}}{U_{sp}\Delta T_{m,sp}} \tag{B14}$$

B.1.1.2. Preheater zone. The overall heat transfer coefficient U_{pr} and the area of the preheater zone, A_{pr}, are computed in a way similar with that used for the superheater.

B.1.1.3. Boiler zone. For the working fluid side in the boiler zone, the Nusselt number is expressed as [33]:

$$Nu_b = (1 + 1.8Xtt^{-0.87})Nu_{s,ph} \tag{B15}$$

where $Nu_{s,ph}$ is the single phase Nusselt number, which is defined by the Dittus-Boelter correlation [31]:

$$Nu_{s,ph} = 0.023Re_L^{0.8}Pr_L^{0.4} \tag{B16}$$

and Xtt is known as the Martinelli factor, which depends on the quality x of the working fluid, as follows [33]:

$$Xtt = \left(\frac{1-x}{x}\right)^{0.9}\left(\frac{\rho_v}{\rho_L}\right)^{0.5}\left(\frac{\mu_L}{\mu_v}\right)^{0.1} \tag{B17}$$

Re_L in Eq. (B16) is the Reynolds number for the liquid in the mixture, which can be expressed as:

$$Re_{ref,b} = \frac{\dot{m}_{ref} d_i (1-x)}{Ac_{ref}\mu_{ref,L}} \tag{B18}$$

Then, heat transfer coefficient in the boiler zone is given by:

$$H_{ref,b} = Nu_b\left(\frac{K_{ref,L}}{d_i}\right) \tag{B19}$$

The heat transfer coefficient in the boiler zone is dependent on the quality of the working fluid mixture (see Eqs. (B15)–(B19)). The quality ranges from x = 0.01 to 0.99 along the boiler zone. The average heat transfer coefficient in the boiler zone is calculated as follows. The boiler zone is divided into fifty equal parts and for each part the heat transfer coefficient is computed. The average value of the heat transfer coefficient is computed as the arithmetic mean of these fifty parts:

$$\overline{H_{ref,b}} = \frac{\sum_{i=1}^{50} H_{ref,b,i}}{50} \quad (B20)$$

On the flue gas side, the Reynolds number is given by:

$$Re_{g,b} = \frac{\dot{m}_g d_h}{Ac_g \mu_{g,b}} \quad (B21)$$

If the flow is laminar ($Re < 2300$) and fully developed, the following equation is used:

$$H_{g,b} = 4.36\left(\frac{K_{g,b}}{d_h}\right) \quad (B22)$$

If $Re > 4000$ the flow is turbulent and the equation to be used is:

$$H_{g,b} = \frac{\frac{f_{g,b}}{8}(Re_{g,b} - 1000)Pr_{g,b}}{1.07 + 12.7\left(\frac{f_{g,b}}{8}\right)^{0.5}Pr_{g,b}^{\frac{2}{3}} - 1}\left(\frac{K_{g,b}}{d_h}\right) \quad (B23)$$

where

$$f_{g,b} = \frac{1}{(0.79\ln(Re_{g,b}) - 1.64)^2} \quad (B24)$$

Then:

$$U_b = \frac{H_{ref,b} \cdot H_{g,b}}{H_{ref,b} + H_{g,b}} \quad (B25)$$

$$A_b = \frac{\dot{Q}_b}{U_b \Delta T_{m,b}} \quad (B26)$$

where U_b and A_b are the overall heat transfer coefficient and the area of the boiler zone, respectively.The total heat transfer area of the evaporator, A_e, is obtained as follows:

$$A_e = A_{sp} + A_b + A_{pr} \quad (B27)$$

B.1.2. Condenser

The processes that take place in the condenser begin in a dry wall desuperheating zone, followed by a wet wall desuperheating zone, then a saturated condensation zone and finally a liquid subcooling zone. The condensation heat transfer coefficient is a strong function of the local vapor quality, increasing as the vapor quality increases [34].

In the condenser, the working fluid flows in the outer tube and the cooling water flows in the inner tube. The condenser can be subdivided into two zones, the desuperheater and the condensation zones, respectively, as shown in Fig. B2. Details for each zone follow.

B.1.2.1. Desuperheater zone. For the cooling water side in the desuperheater zone at the outer tube, the Reynolds number is defined as:

$$Re_{w,des} = \frac{\dot{m}_w d_h}{Ac_g \mu_{w,des}} \quad (B28)$$

If the flow is laminar ($Re < 2300$) and fully developed, then the following equation may be used to compute the heat transfer coefficient:

$$H_{w,des} = 4.36\left(\frac{K_{w,des}}{d}\right) \quad (B29)$$

If $Re > 4000$ the flow is turbulent and the equation to be used is:

$$H_{w,des} = \frac{\frac{f_{w,des}}{8}(Re_{w,des} - 1000)Pr_{w,des}}{1.07 + 12.7\left(\frac{f_{w,des}}{8}\right)^{0.5}Pr_{w,des}^{\frac{2}{3}} - 1}\left(\frac{K_{w,des}}{d}\right) \quad (B30)$$

where

$$f_{w,des} = \frac{1}{(0.79\ln(Re_{w,des}) - 1.64)^2} \quad (B31)$$

The condensation inside tube is a more complicated process, since it is strongly influenced by the vapor velocity and the rate of liquid accumulation on the walls of the tubes. For the working fluid side in the inner tube for the heat exchanger, the Reynolds number can be defined as follows:

$$Re_{ref,des} = \frac{\dot{m}_{ref} d_i x_c}{Ac_f \mu_{ref,des}} \quad (B32)$$

where $\mu_{ref,des}$ is the average value of kinematic velocity of working fluid between T_4 and T_{ev}.

Two cases denoted below A and B are possible, depending on fluid velocity.

A. $Re_{ref,des} < 35{,}000$

The Dobson & Chato correlation may be used [35]:

$$H_{ref,des} = 0.555\left(\frac{g\rho_L(\rho_L - \rho_V)K_{ref,des,L}^3 h_{fgm}}{\mu_{ref,des,L}(T_{sat} - T_p)d_i}\right)^{0.25} \quad (B33)$$

where g is the gravitational acceleration, ρ_L and ρ_V are liquid and vapor mass densities of the working fluid, respectively, $K_{ref,des,L}$ is the thermal conductivity of the working fluid in liquid phase, $\mu_{ref,L}$ is the kinematic viscosity of the working fluid in liquid phase. Also, the modified specific latent heat of evaporation (h_{fgm}) is a function of the specific latent heat (h_{fg}) of the working fluid, as given in the following equation:

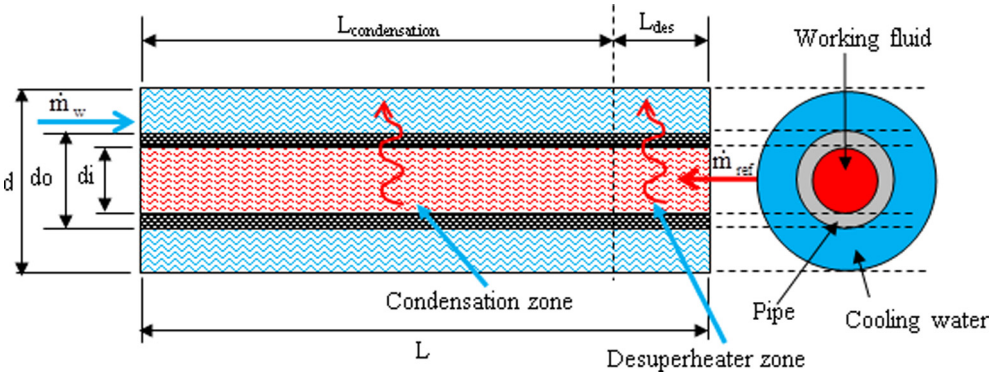

Fig. B2. Condenser representation.

$$h_{fgm} = h_{fg} + \frac{3}{8} C_{P_L} (T_c - T_p) \quad \text{(B34)}$$

Here C_{p_L} is the specific heat of the working fluid in liquid phase, T_c is the saturation temperature of the working fluid, T_p is the surface wall temperature.

B. $Re_{ref,des} \geq 35{,}000$

The Boyko & Kruzhilin correlation may be used [36]:

$$H_{ref,des} = 0.021 \left(\frac{K_{ref,des,L}}{d_i} \right) Re^{0.8}_{ref,des,L} Pr^{0.43}_{ref,des,L} \left[1 + x \left(\frac{\rho_L}{\rho_V} - 1 \right) \right]^{0.5} \quad \text{(B35)}$$

In the desuperheater zone, the overall heat transfer coefficient U_{des} is expressed as:

$$U_{des} = \frac{H_{ref,des} \cdot H_{w,des}}{H_{ref,des} + H_{w,des}} \quad \text{(B36)}$$

and the area of the desuperheater zone is given by:

$$A_{des} = \frac{\dot{Q}_{des}}{U_{des} \Delta T_{m,des}} \quad \text{(B37)}$$

B.1.2.2. The condensation zone. The overall heat transfer coefficient, $U_{condensation}$, and the area of the condensation zone, $A_{condensation}$, are computed in a way similar to that used for the desuperheater zone

The total heat transfer area of the condenser is obtained as follows:

$$A_{con} = A_{condensation} + A_{des} \quad \text{(B38)}$$

References

[1] Jadhao JS, Thombare DG. Review on exhaust gas heat recovery for I.C. Engine. Int J Eng Innovative Technol 2013;2:93–100.
[2] Turboden, Turboden ORC plants for Industrial Heat Recovery. <http://www.turboden.eu/en/public/downloads/12-COM.P-21-rev.23.pdf>; 2015.
[3] Iacopo V, Agostino G. Internal combustion engine (ICE) bottoming with Organic Rankine cycles (ORCs). Energy 2010;35:1084–93.
[4] Maogang H, Xinxin Z, Ke Z, Ke G. A combined thermodynamic cycle used for waste heat recovery of internal combustion engine. Energy 2011;36:6821–9.
[5] Wang EH et al. Performance analysis of a novel system combining a dual loop organic Rankine cycle (ORC) with a gasoline engine. Energy 2012;43:385–95.
[6] Alberto B. Recovery of exhaust and coolant heat with R245fa organic Rankine cycles in a hybrid passenger car with a naturally aspirated gasoline engine. Appl Therm Eng 2012;36:73–7.
[7] Gequn S, Lina L, Hua T, Haiqiao W, Youcai L. Analysis of regenerative dual-loop organic Rankine cycles (DORCs) used in engine waste heat recovery. Energy Convers Manage 2013;76:234–43.
[8] Huan X, Ming-Jia L, Chao X, Ya-Ling H. Parametric optimization of regenerative organic Rankine cycle (ORC) for low grade waste heat recovery using genetic algorithm. Energy 2013;58:473–82.
[9] Guopeng Y, Gequn S, Hua T, Haiqiao W, Lina L. Simulation and thermodynamic analysis of a bottoming Organic Rankine Cycle (ORC) of diesel engine (DE). Energy 2013;51:281–90.
[10] Tianyou W et al. Comparisons of system benefits and thermo-economics for exhaust energy recovery applied on a heavy-duty diesel engine and a light-duty vehicle gasoline engine. Energy Convers Manage 2014;84:97–107.
[11] Gequn S, Lina L, Hua T, Haiqiao W, Guopeng Y. Parametric and working fluid analysis of a dual-loop organic Rankine cycle (DORC) used in engine waste heat recovery. Appl Energy 2014;113:1188–98.
[12] Jian S, Chun-wei G, Xiaodong R. Parametric design and off-design analysis of organic Rankine cycle (ORC) system. Energy Convers Manage 2016;112:157–65.
[13] Prisecaru T, Dobrovicescu A, Petcu C, Apostol V, Prisecaru M, Popescu G, et al. Experimental Investigation of Waste Heat Available for a Hybrid Micro-Cogeneration Group Involving a Diesel Engine Electric Generator and Organic Rankine Cycle. Appl Mech Mater 2014;659:440–5.
[14] Research Grant". Hybrid micro-cogeneration group of high efficiency equipped with an electronically assisted ORC", founded by Executive Agency for Higher Education, Research. Development and Innovation Funding of Romania, Grant Code: PN-II-PT PCCA-2011-3.2-0059, Grant No.: 75/2012.
[15] Bernardo P, Joaquín NE, Francisco M. Bottoming organic Rankine cycle configurations to increase internal combustion engines power output from cooling water waste heat recovery. Appl Therm Eng 2013;61:364–71.
[16] Engineering Equation Solver, Academic commercial V.9.914, #2538 Faculty of Mechanical Engineering, University Politehnica of Bucharest. <http://www.fchart.com/ees/>; 2016 [accessed 01.06.2016].
[17] Junjiang B, Li Z. A review of working fluid and expander selections for organic Rankine cycle. Renew Sustain Energy Rev 2013;24:325–42.
[18] Fu BR, Liu CH. Performance of a 250 kW organic Rankine cycle system for off-design heat source conditions. In: 1st International E-Conference on Energies 2014, Conference Proceedings Paper – Energies, p. 14–31.
[19] Pănoiu N. Steam boilers. Bucharest: Didactică și pedagogică; 1982.
[20] Naijun Z, Xiaoyuan W, Zhuo C, Zhiqi W. Experimental study on organic Rankine cycle for waste heat recovery from low-temperature flue gas. Energy 2013;55:216–25.
[21] Zhang HG, Wang EH, Fan BY. Heat transfer analysis of a finned-tube evaporator for engine exhaust heat recovery. Energy Convers Manage 2013;65:438–47.
[22] Charles S, Christopher D. Review of organic Rankine cycles for internal combustion engine exhaust waste heat recovery. Appl Therm Eng 2013;51:711–22.
[23] Bertrand FT, Lambrinos Gr, Frangoudakis A, Papadakis G. Low-grade heat conversion into power using organic Rankine cycles – A review of various applications. Renew Sustain Energy Rev 2011;15:3963–79.
[24] You-Rong L, Mei-Tang D, Chun-Mei W, Shuang-Ying W, Chao L. Potential of organic Rankine cycle using zeotropic mixtures as working fluids for waste heat recovery. Energy 2014;77:509–19.
[25] Hua T, Gequn S, Haiqiao W, Xingyu L, Lina L. Fluids and parameters optimization for the organic Rankine cycles (ORCs) used in exhaust heat recovery of internal combustion engine (ICE). Energy 2012;47:125–36.
[26] Iacopo V, Agostino G. Internal combustion engine (ICE) bottoming with organic Rankine cycles (ORCs). Energy 2010;35:1084–93.
[27] Aboaltabooq MHK, Prisecaru T, Pop H, Apostol V, Prisecaru M, Popescu Gh, et al. Effect of variable heat input on the heat transfer characteristics in an Organic Rankine Cycle system. Renew Energy Environ Sustain 2016;1:13.
[28] Mojtaba T, Saeed J, Mojtaba B. A comprehensive study on waste heat recovery from internal combustion engines using organic Rankine cycle. Therm Sci 2013;17(2):611–24.
[29] Mago PJ, Chamra LM, Somayaji C. Performance analysis of different working fluids for use in organic Rankine cycles. Power Energy 2006;221:255–64.
[30] Angad SP. Study of organic Rankine cycle systems with the expansion process performed by twin screw machines Doctoral thesis. London: City University; 2012.
[31] Vargas JVC, Ordonez JC, Bejan A. Power extraction from a hot stream in the presence of phase change. Int J Heat Mass Transf 2000;43:191–201.
[32] Musbaudeen OB, Eray U. Numerical analysis of an organic Rankine cycle under steady and variable heat input. Appl Energy 2013;107:219–28.
[33] Qicheng C, Jinliang X, Hongxia C. A new design method for organic Rankine cycles with constraint of inlet and outlet heat carrier fluid temperatures coupling with the heat source. Appl Energy 2012;98:562–73.
[34] Dominik M, Christoph W, Hartmut S. Effect and comparison of different working fluids on a two-stage organic Rankine cycle (ORC) concept. Appl Therm Eng 2014;63:246–53.
[35] Bergman TL, Lavine AS, Incropera FP, Dewitt DP. Fundamentals of heat and mass transfer. 7th ed. USA: John Wiley & Sons; 2011.
[36] Ghazi M, Ahmadi P, Sotoodeh AF, Taherkhani A. Modeling and thermo economic optimization of heat recovery heat exchangers using a multimodal genetic algorithm. Energy Convers Manage. 201;58:149–156.